

Zinc and Silver Salts-Containing Lamellar Titanium Phosphate: A Multifunctional Filler

Enzo Erbisti Garcia, Gerson Alberto Valencia Albitres, Daniela França Silva Freitas, Danielle Mattos Mariano, Luis Cláudio Mendes*

Universidade Federal do Rio de Janeiro, Instituto de Macromoléculas Professora Eloisa Mano, Avenida Horácio Macedo, Rio de Janeiro, Brazil

Email: *lcmendes@ima.ufrj.br

How to cite this paper: Garcia, E.E., Albitres G.A.V., Freitas, D.F.S., Mariano, D.M. and Mendes, L.C. (2022) Zinc and Silver Salts-Containing Lamellar Titanium Phosphate: A Multifunctional Filler. *Materials Sciences and Applications*, 13, 366-388. <https://doi.org/10.4236/msa.2022.136021>

Received: May 2, 2022

Accepted: June 17, 2022

Published: June 20, 2022

Copyright © 2022 by author(s) and Scientific Research Publishing Inc. This work is licensed under the Creative Commons Attribution International License (CC BY 4.0).

<http://creativecommons.org/licenses/by/4.0/>



Open Access

Abstract

Zinc and silver compounds have been studied because they have ultraviolet light barrier properties and bactericidal action, respectively. Materials with multifunctional characteristics have been sought to produce polymeric nanocomposites. In this work, the chemical modification of titanium phosphate (TiP) was carried out through a route with successive intercalations. TiP was synthesized and consecutively pre-expanded with ethylamine and pyromellitic acid. Then it was modified with zinc acetate and silver nitrate. The final product was characterized by Fourier transform infrared spectroscopy, differential scanning calorimetry, wide-angle X-ray diffractometry, field emission scanning electron microscopy coupled with energy dispersive X-ray spectroscopy and thermogravimetry. Infrared revealed dislocation and appearance of bands according to the intercalating agent. Inorganic salts interfered in the crystallization and melting processes of pyromellitic acid. Vanishing of the TiP *hkl* plane and variation and appearance of new crystallographic planes at low diffraction angles induced intercalation. SEM showed agglomerated structures. New thermal degradation events at higher temperatures endorsed the formation of zinc and silver carboxylate salts. We concluded that a new miscellaneous and multifunctional matter was achieved.

Keywords

Titanium Phosphate, Intercalation, Pyromellitic Acid, Zinc Acetate, Silver Nitrate, Ethylamine

1. Introduction

Nanotechnology has opened new horizons in Material Science and Technology.

It also allowed the interconnection between the different areas of knowledge. The change from micrometer to nanometer scale exacerbated properties in several organic and inorganic compounds.

Zinc and silver nanoparticles are interesting since they possess a large surface area and several unusual properties such as non-toxicity, availability, stability, and strong antimicrobial activity. One of the best routes to take advantage of these properties is by mixing these nanoparticles with polymers to obtain nanocomposites. The aggregation of features builds a matter with functionalities of both components [1] [2] [3]. There are several articles devoted to polymer nanocomposites containing zinc oxide (ZnO). The latter possesses low cost, easy availability, intense ultraviolet absorption, antibacterial action and so on [4] [5].

Li *et al.* prepared by solution casting polyurethane membranes embedded with zinc oxide nanoparticles. The authors reported UV-shielding properties at high temperature [6]. Thin film of novel kind of thermoplastic elastomer—polyether block amide, PEBA—filled with different concentrations of ZnO was investigated by Sheikh and collaborators. It was found the great increase in the T_g from -51.9°C to 3.06°C with the addition of 0.5 wt% of ZnO [7]. ZnO-modifying surface of polyamide 6, poly (ethylene terephthalate) and polypropylene textiles was studied by Fiedot-Toboła and co-authors. Significant bactericidal activity was reported. Gram-negative *E. coli* was more sensitive to ZnO and after 5 h of cells incubation with the textiles resulted in lethal effect. Opposite behavior of Gram-positive *S. aureus* needed longer contact time to obtain the same effect [8].

Few studies on polymer composites with zinc acetate were found. Zhou *et al.* prepared zinc acetate-polyethylene composite coatings synthesized in vacuum by electron beam dispersion method with pulse laser assistant. They evaluated coating photoluminescence features with respect to the laser assistant and post-annealing temperature (100°C - 200°C). At 200°C , the annealed zinc acetate-polyethylene coating exhibited absorption of ZnAc at 361 nm. According to the authors, the complete decomposition of zinc acetate and carbonate occurred at 200°C producing ZnO [9].

Since ancient times, silver has been known due to its antibacterial action. Nowadays, in several sectors of human activities, the application of silver as bacterial attack controller has been grown. Even a low concentration, silver ions present efficacy against microorganisms like bacteria, yeast, fungi, and viruses but low toxicity to human cells [4].

Sionkowska, *et al.* studied nanocomposites based on collagen/chitosan blends embedded with silver nanoparticle. Micrograph of blend films revealed the aggregation of the silver particles in the range of 0.2 - 2 μm [10]. Searching inhibition of bacteria growth, Rajabi *et al.* impregnated poly (ethylene terephthalate) (PET) fabric with silver oxide. The highest inhibitory efficiency was attained at pH = 8.5 [11].

Titanium and Zirconium are metals included in the Group 4 of the Periodic Table. Some their compounds have been used to synthesize lamellar phosphates.

Their phosphates show broad potential of usage as catalyst, ion-exchange and when their interlayer spacing are chemically modified found application as fillers in polymer composites building devices with features such as proton conduction, drug delivery, energy storage, sensors and biosensors, flame retardants and so on [12] [13] [14]. Titanium and zirconium phosphates show narrow interlayer distance. In general, their use as fillers in polymeric composites need the expansion of their galleries efficiently achieved with amines [15]. The first report on cation exchange properties of α -zirconium phosphate, α -ZrP, happened in 1956 [16]. Only about one decade later, the investigations on α -titanium phosphate, α -TiP, started. The main characteristic reported was the higher ability of α -TiP to undergo ion exchange [17]. Many studies focused on its functionalization through the intercalation with amines and its exfoliation leading to several potential applications [18] [19] [20].

García-Glez, *et al.* studied crystalline α -phases of zirconium and titanium phosphates synthesized via hydrothermal route and afterwards surface-enriched with silver nanoparticles. The EDX analyses revealed that α -TiP gained on average double of the silver content as compared to zirconium counterparts. Both Ag-enriched metal phosphates showed antibacterial properties. The same minimum inhibitory concentration (MIC) and minimum bactericidal concentration (MBC) was found for both Ag-enriched metal phosphates [21] [22]. Photocatalyst based on pristine titanium phosphate and modified one with AgNO₃ and NaBr producing hybrids AgBr@Ag/Titanium Phosphate was performed by Ren and co-authors. Four samples with different AgBr@Ag/TP mass ratios (20%, 100%, 150%, 200%) were obtained by the authors, and were labeled as AgBr@Ag/TP-1, AgBr@Ag/TP-2, AgBr@Ag/TP-3, AgBr@Ag/TP-4. Pristine TiP did not show absorption in the visible light region while AgBr@Ag/TP-3 had better absorption performance. It was detected that when the addition of AgBr@Ag exceeded a critical value an agglomeration emerged, and the absorption ability decreased [23].

The purpose of this work was built a matter which could have jointly the properties of zinc and silver compounds. Thereby, using the expertise of our research group on synthesis and intercalation of lamellar phosphates, we experienced the intercalation of titanium phosphate with zinc acetate and silver nitrate. The pyromellitic acid was also intercalated searching compatibilization with aromatic polymer in future work. Structural, crystallographic, thermal, and morphologic aspects were investigated. The final product is miscellaneous and multifunctional matter.

2. Experimental

2.1. Materials

Table 1 arranges the selected materials.

2.2. Titanium Phosphate (TiP) Synthesis

The titanium isopropoxide was dropped to the phosphoric acid (1:8 molar ratio)

Table 1. Materials and characteristics.

Material	Characteristics	Origin
Phosphoric acid	H ₃ PO ₄ , 85% wt./mL	Sigma-Aldrich
Titanium isopropoxide	C ₁₂ H ₂₈ O ₄ Ti, 97%, molar mass = 284.22 g/mol	Sigma-Aldrich
Ethanol	C ₂ H ₆ O, 99% molar mass = 46 g/mol	Sigma-Aldrich
Ethylamine	C ₂ H ₅ NH ₂ , 70%, density = 0.81 g·mL ⁻¹	Sigma-Aldrich
Pyromellitic acid	C ₁₀ H ₆ O ₈ 96% Melting point = 281 °C - 285 °C	Sigma-Aldrich
Zinc acetate	ZnAc, Molar mass = 219.51 g/mol	Sigma-Aldrich
Silver nitrate	AgNO ₃ , Molar mass = 169.89	Isofar

under vigorous stirring, following the addition of deionized water, at 120 °C, for 24 hours. After that, the reactional medium was washed with deionized water until attaining pH = 6 and finally dried in an oven, at 90 °C, until constant weight. The final product was labeled as TiP [20] [24] [25].

2.3. Intercalation of the TiP with Ethylamine, Pyromellitic Acid, Zinc Acetate and Silver Nitrate

Successively, TiP was intercalated with four different matters. The first intercalation was performed dropping an ethanolic solution of ethylamine onto ethanolic dispersion of TiP, at 30 °C, under stirring, for 24 hours. The reaction medium was washed with deionized water until pH around 6 was attained. The dispersion was dried in an oven, at 90 °C, up to reach constant weight. It was labeled as TiP/EA. Following, TiP/EA was submitted to the intercalation using pyromellitic acid. Ethanolic solution of that acid was dropped onto ethanolic dispersion of TiP/EA, at 30 °C, under stirring, for 24 hours. The medium was dried in an oven, at 90 °C, until to achieve constant weight. It was labeled as TiP/EA/AP. The latter underwent chemical modification with ZnAc. Ethanolic solution of zinc salt was dropped onto ethanolic dispersion of TiP/EA/AP, at 30 °C, under stirring, for 4 hours. The dispersion was dried at 90 °C until constant weight. It was assigned as TiP/EA/AP/Zn. Finally, aqueous solution of AgNO₃ was added to the aqueous dispersion of TiP/EA/AP/Zn, at 30 °C, under stirring, for 4 hours. After drying, at 90 °C, for 24 hours and constant weight, the final product received the acronym TiP/EA/AP/Zn/Ag. Schematically, **Figure 1** presents all steps of synthesis and intercalations.

2.4. Fourier Transform Infrared Spectroscopy (FTIR)

Infrared evaluation was performed in a Perkin-Elmer equipment, model Frontier MIR/FIR, within the range of 4000-400 cm⁻¹. The spectra were obtained by attenuated total reflectance (ATR), using 60 scans and resolution of 4 cm⁻¹.

2.5. Differential Scanning Calorimetry (DSC)

Hitachi DSC 700 was used for DSC analysis, following ASTM D3418 [26]. Three

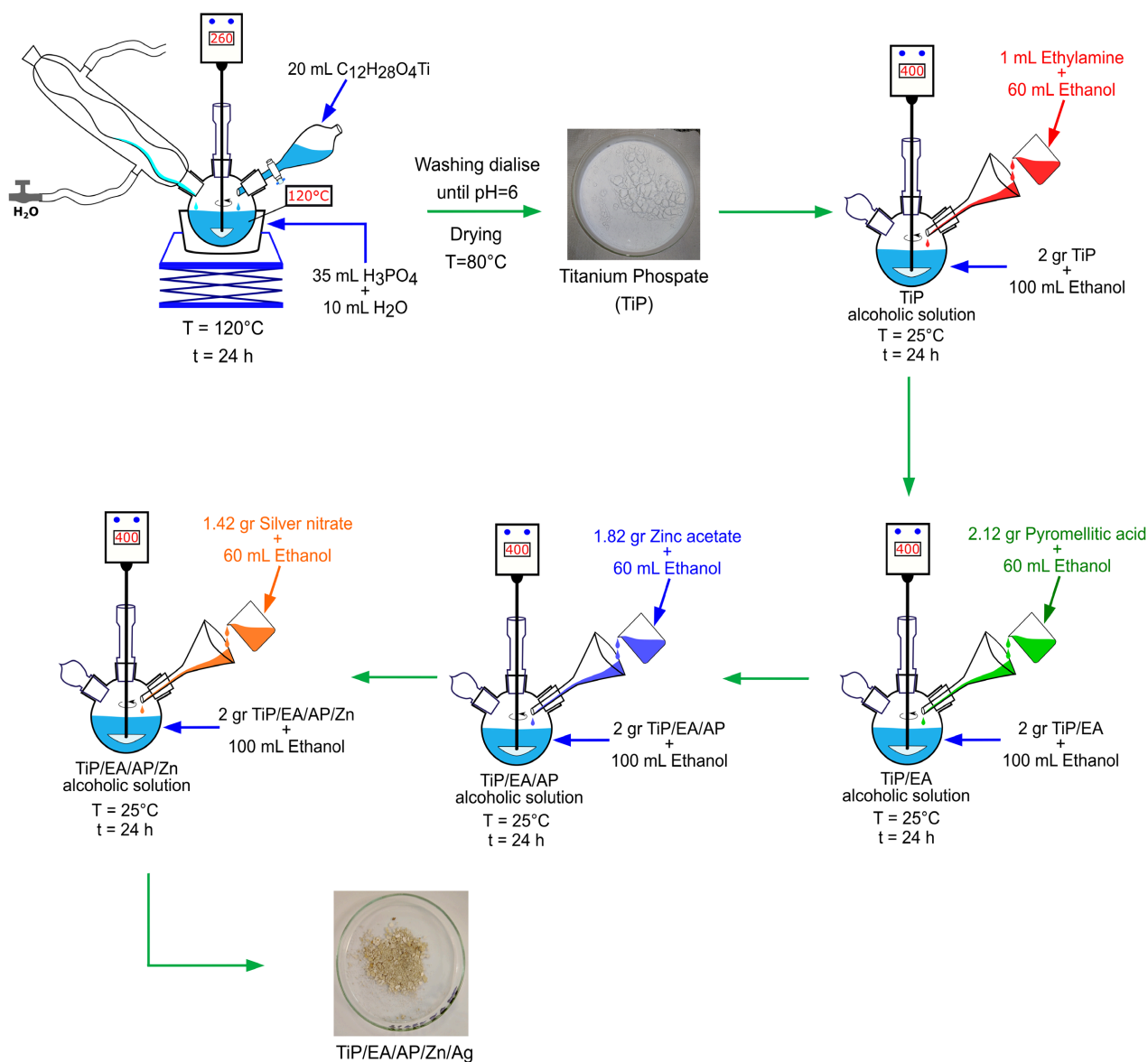


Figure 1. Schematic representation of the synthesis and chemical modification of TiP.

thermal cycles were performed. Firstly, a heating cycle was conducted from 20-300°C, at $10^\circ C \cdot min^{-1}$, in nitrogen atmosphere, keeping for 2 minutes to eliminate the thermal history. Following, a cooling cycle at high thermal rate (quenching) was experienced. Finally, a third cycle was accomplished at the same conditions applied in the first one. Crystallization (T_c) and melting (T_m) temperatures besides melting enthalpy (ΔH_m , $J \cdot mg^{-1}$) were registered.

2.6. Wide Angle X-Ray Diffractometry (WAXD)

The wide-angle X-ray diffraction (WAXD) analysis was performed in a Rigaku Ultima IV diffractometer, with $CuK\alpha$ radiation ($\lambda = 1.5418 \text{ \AA}$) and experimental conditions of 40 kV, 20 mA, step of 0.05, ranging the 2θ angle from 2° to 40° .

2.7. Field Emission Scanning Electron Microscopy/Energy Dispersive X-Ray Spectroscopy (FESEM/EDX)

SEM analysis was performed at Tescan field emission microscope, model MIRA 4 LMU, cannon FEG Schottky (Field Emission Scanning Electron Microscope). The SEM has as an accessory an EDX detector with a 30 mm² Si₃N₄ window and a resolution lower than 129 eV for the MnK α emission line. The samples were coated with fine gold layer and the micrographs were taken. The elemental analysis was monitored by EDX.

2.8. Thermogravimetry (TGA)

Thermogravimetry was conducted in TA analyzer model Q500, from 30 to 700°C, at 10°C·min⁻¹, under nitrogen atmosphere. The thermal degradation steps were registered through the loss mass and its derivative curves.

3. Results and Discussion

3.1. Infrared Spectroscopy

Table 2 arranged the main absorption bands of the precursors and phosphates.

Table 2. Infrared absorptions of precursors and phosphates.

Sample	Infrared absorption bands (cm ⁻¹)
ZnAc	3090, 3163, 1719, 1562, 1569, 1449, 1408, 1385, 1056, 1020, 954, 851, 732, 696, 623
AgNO ₃	3358, 3483, 2428, 1763, 1630, 1763, 1385, 1378, 839, 824, 800
Pyromellitic acid	3535, 3402, 3131, 3058, 1714, 1697, 1651, 1508, , 1442, 1410, 1306, 1275, 1264, 1141, 1118, 959, 926, 882, 818, 800, 765, 753, 718, 653, 581, 499, 466, 429
TiP	3554, 3476, 1621, 1617, 1615, 1640, 1646, 1728, 1799, 1528, 1033, 1255, 1179, 1115, 1072, 1044, 1033, 1013, 970, 879, 714, 615, 542, 524, 486, 423, 403
TiP/EA	3423, 3537, 3062, 2986, 1736, 1634, 1597, 1469, 1462, 1398, 1376, 1364, 1332, 1221, 1187, 1126, 1040 1002, 967, 958, 927, 792, 782, 632, 522, 461, 418
TiP/EA/AP	3458, 3192, 3065, 1795, 1728, 1702, 1662, 1629, 1597, 1522, 1511, 1468, 1422, 1398, 1325, 1264, 1215, 1113, 1042, 946, 957, 828, 794, 792, 651, 619, 1722, 1701, 1687, 1596, 1512, 1467, 1399, 1325, 1264, 1214, 1113, 1041, 957, 946, 828, 651, 620, 794, 792, , 525, 503, 468, 435, 417
TiP/EA/AP/Zn	3566, 3444, 3201, 1757, 1636, 1607, 1563, 1545, 1490, 1476, 1455, 1398, 1384, 1367, 1221, 1140, 1040, 988, 976, 959, 869, 819, 796, 765, 649, 619, 547, 526, 484, 468, 410
TiP/EA/AP/Zn/Ag	3455, 3227, 1764, 1628, 1604, 1563, 1548, 1496, 1418, 1385, 1372, 1322, 1272, 1219, 1143, 1129, 1041, 1002, 986, 969, 950, 868, 821, 762, 709, 631, 544, 533, 519, 476, 428

For ZnAc, bands at 3090, 3163, 1563, 1449, 1020, 954, 696 and 623 cm^{-1} were highlighted. They find consensus with those published by Pouchert [27]. The bands at 1562, 1569 cm^{-1} represented the stretching vibration of O=C=O group. Bands at 3358, 3483, 2428, 1763, 1385, 824 cm^{-1} were registered in the spectrum of AgNO_3 , Augustine *et al.* in their work on green synthesis of silver nanoparticles attributed the band at 1385 cm^{-1} as nitro compounds symmetric vibrations [28]. Pyromellitic exposed several absorptions. Bands at 3532, 3402 and 3131 cm^{-1} were associated to the intramolecular and intermolecular hydrogen bonds, respectively. Aryl =C-H stretching was registered at 3058 cm^{-1} . Carbonyl symmetric stretching emerged from 1714, 1697 and 1651 cm^{-1} . Aryl C=C stretching occurred at 1508 and 1442 cm^{-1} . Band at 1410 cm^{-1} revealed O=C=O stretching. Bands at 1275, 1264, 1141 and 1118 cm^{-1} could be associated to the O=C=O and C-H asymmetric vibrations of aryl acid [29]. Vibrations related to the ortho disubstituted aromatic ring, C-H out of plane and O=C=O bending were associated to the bands at 959, 926, 882, 818, 800, 765, 753, 718, 653, 581, 499, and 466 cm^{-1} [29] [30] [31] [32]. For TiP, absorptions around 3554 and 3476 cm^{-1} were imputed to the symmetric and asymmetric stretching of hydrogen bond between P-O-H groups and adsorbed water. At 1617 cm^{-1} , H-O-H vibration of the water constricted at crystalline lattice. Vibrations at 1255, 1115, 1033, 1013, 970 cm^{-1} were ascribed to the P-O_4^- , P-O and P-O-H stretching. Bands at 615, 542, 524 and 423 cm^{-1} attributed to the vibrations of P-O-H and Ti-O moieties. After intercalation with ethylamine, there were band shift and new ones. The previous bands at 3000-4000 cm^{-1} were shifted to 3423 and 3062 cm^{-1} on account of the formation of $\text{PO}_4^- \text{ } ^+\text{HN-CH}_2\text{CH}_3$ amine salt. New bands at 2986 cm^{-1} (CH_2 amine stretching), 1469 cm^{-1} (CH_2 amine stretching) and 1376 cm^{-1} (CH_3 amine stretching) appeared owing to the amine insertion. In the region between 1200-400 cm^{-1} , the vibrations referred to the phosphate and Ti-O moieties were displaced to lower wavelength 1002, 967, 927, 792, 632, 522, 461 and 418 cm^{-1} . These findings are in accordance with published elsewhere [20] [33] [34]. With the consecutive addition of pyromellitic acid, ZnAc and AgNO_3 , the spectra featured the combination of the constituent's signals. For better viewing, **Figure 2** shows the deconvolution of the spectral region at 1800 - 1500 cm^{-1} (**Figure 2(a)**), 1500 - 1000 cm^{-1} (**Figure 2(b)**) and 1000 - 500 cm^{-1} (**Figure 2(c)**) for TiP/EA/AP, TiP/EA/AP/Zn and TiP/EA/AP/Zn/Ag samples. For TiP/EA/AP, the bands at 3192, 1629, 1042, 957, 651, 619 cm^{-1} were assigned to TiP moieties. Absorptions at 3470 (stretching of hydrogen bond of aryl acid), 1722, 1701 and 1687 cm^{-1} (aryl acid C=O stretching), 1596, 1512 and 1467 cm^{-1} (aryl C=C stretching), 1402 cm^{-1} (aryl acid O=C=O stretching), 1263 and 1215 cm^{-1} (PO_4^- and aryl acid C-H vibrations), 957, 946, 794 cm^{-1} (aryl acid C-H out-of-plane and C-H bending, 828 cm^{-1} (aryl acid O=C=O bending), and 525, 467 and 416 cm^{-1} (vibrations of P-O-H and Ti-O moieties) appeared. TiP/EA/AP/Zn sample showed multiple bands related to all matters involved in the phosphate modification. Some spectral changes could be highlighted. The disappearance of the

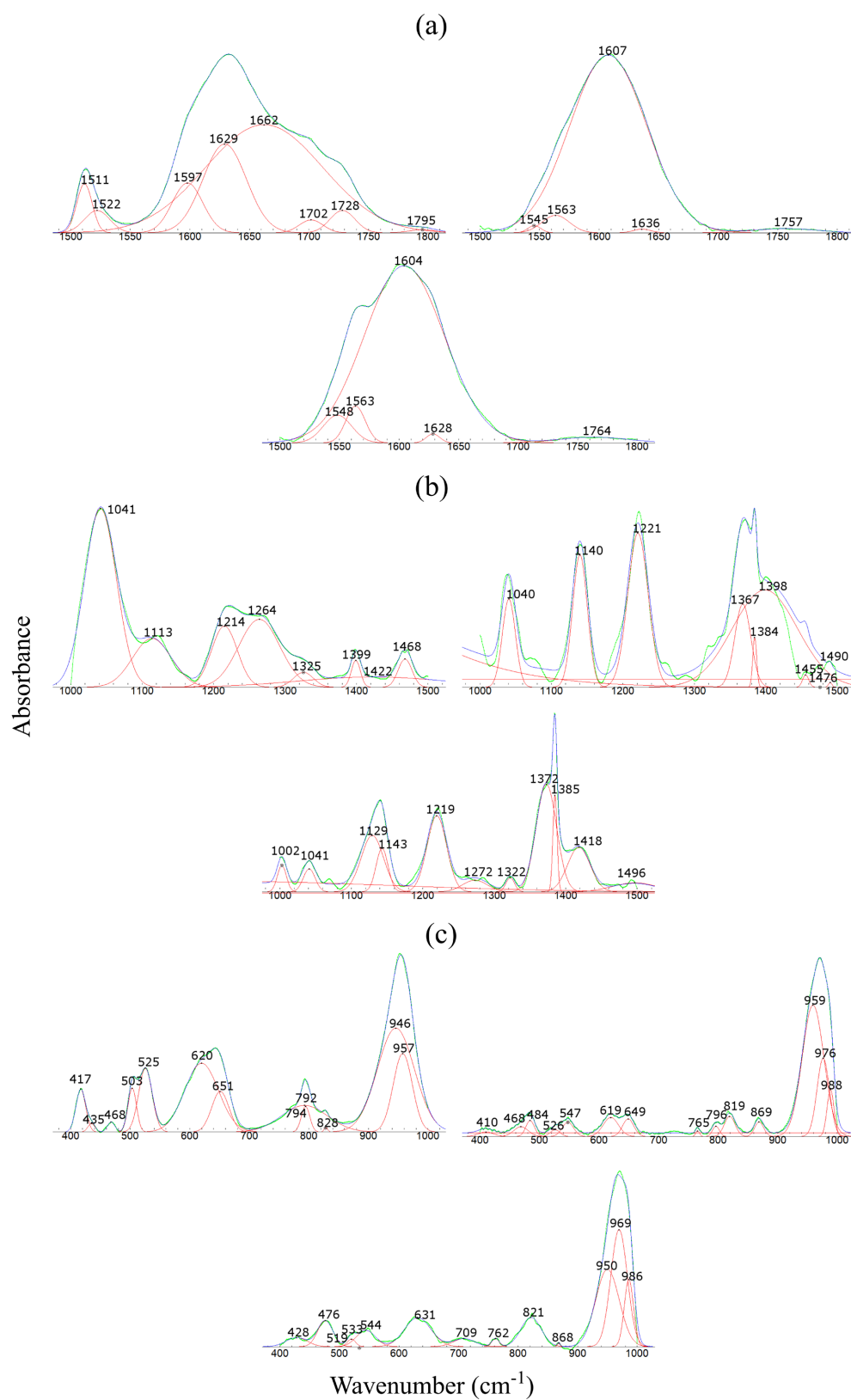


Figure 2. Deconvolution of the spectral region at $1800\text{--}1500\text{ cm}^{-1}$ (**Figure 2(a)**), $1500\text{--}1000\text{ cm}^{-1}$ (**Figure 2(b)**) and $1000\text{--}500\text{ cm}^{-1}$ (**Figure 2(c)**) for TiP/EA/AP, TiP/EA/AP/Zn and TiP/EA/AP/Zn/Ag samples.

aryl acid bands at 1714, 1697, 1651 cm^{-1} . New bands are arising at 1563, 1545, 1367 and 1384 cm^{-1} . The absorptions between 900-800 cm^{-1} were strongly affected. Yang *et al.* investigated the zinc complexation with pyromellitic acid. They highlighted absorptions at 3390 cm^{-1} (O-H bonds stretching), 3198 cm^{-1} (C-H stretching), 1624 cm^{-1} (O-H stretching water molecules), 1557 and 1406 cm^{-1} (carboxyl asymmetric and symmetric stretching), 625 (C=O bending). Although bands at 1146, 927, 816, 763, and 517 cm^{-1} have been registered their assignments were not reported [35]. Qin *et al.* studied the *in-situ* formation of zinc phthalate as nucleation agent for polypropylene. They pointed out the appearance of bands at 1578 cm^{-1} (COO^- asymmetric stretching) and 1421 cm^{-1} (COO^- symmetric stretching). According to them, when the subtraction of two signals is low bridging bidentate structure can be achieved [36]. Loring *et al.* investigated the infrared of phthalic acid as mono and di-phthalate ions in sodium chloride aqueous solution, at different pH. The study was performed in the spectral region between 1810-975 cm^{-1} . The transformation from phthalic acid to di-phthalate ion revealed the disappearance of aryl acid C=O vibration, dislocation and overlapping of some infrared signals. Bands at 1686 cm^{-1} (O-H bending of hydration water), 1604 and 1584 cm^{-1} (C=C stretching), 1555 cm^{-1} (CO_2^- asymmetric stretching), 1487 and 1445 cm^{-1} (C=C stretching), 1405 and 1382 cm^{-1} (CO_2^- symmetric stretching), 1291 cm^{-1} (C-H bending), 1266 cm^{-1} (C=C stretching), 1166, 1150 and 1134 cm^{-1} (C-H bending), 1087 cm^{-1} (C=C bending) and 1040 cm^{-1} (C=C stretching) were highlighted [37]. When AgNO_3 was added, the TiP/EA/AP/Zn/Ag spectrum also showed changes in the different spectral regions. Suh, *et al.* and Joo, *et al.* investigated the adsorption of series of aryl substituted acids on silver colloidal by means of surface-enhanced Raman spectroscopy [38] [39]. The data of Suh and collaborators induced to conclude that three types of carboxylate groups surface geometry could have emerged. They focused their proposition on the relative intensity of the bands related to COO^- stretching (between 1400 - 1350 cm^{-1}) and COO^- bending (between 850-800 cm^{-1}). Flat geometry was proposed when COO^{2-} reacted through its π -electrons and COO^- stretching showed higher intensity than its bending counterpart. When the tilting of COO^- with respect the surface increases the relative intensity of COO^- bending vibration increases as compared to the stretching one leading to the reaching of two-legged surface. In the third consideration, bending absorption is stronger than its stretching counterpart conducted to the one-legged geometry. Joo, *et al.* built their work on the adsorption of phthalic acid onto silver surface under varying pH. They pointed out that phthalic molecules interacted with silver as dicarboxylate. High pH induced high degree of tilting of phthalic structure. It was presumed the occurrence of simultaneous σ and π -coordination owing to steric hindrance and electrostatic repulsion between two carboxylates groups. In summary, we believed that TiP was chemically modified in each intercalation step. The addition of ethylamine induced an acid-base reaction forming an amine salt as $\text{PO}^- \text{ } ^+_3\text{HN-CH}_2\text{CH}_3$ and free amine. When the pyromellitic acid was put in we noticed the absence of the imide bands at

3205, 1774 and 1745 cm^{-1} indicating no reaction between free ethylamine and acid [40]. After ZnAc addition, the presence of the band at 1563 cm^{-1} was associated to the stretching of COO^- group of the free zinc acetate. The new band was detected at 1545 cm^{-1} was understood as the formation of zinc carboxylate. The pair of bands found at 1384/1367 were ascribed to COO^- stretching of pristine ZnAc and zinc carboxylate, respectively. The band at 819 cm^{-1} encompassed acid vibrations at 826 and 816 cm^{-1} plus COO^- bending of zinc salt, pristine and that arising from pyromellitic acid. Afterward AgNO_3 addition, the bands at 1548 and 1367 were shifted to 1545 and 1372 cm^{-1} . Their assignments were like those observed after zinc salt addition. Likewise, the band at 821 cm^{-1} wrapped infrared signals related to the acid and COO^- vibrations of zinc and silver carboxylate salts. The careful observation on zinc nitrate absorptions (3576, 3485, 1638, 1384, 828, 642 cm^{-1}) and silver acetate (3341, 2926, 1562, 1406, 1340, 1120, 1026, 1018, 920, 647, 622, 482 cm^{-1}) it could be hypothesized that ion exchange could have occurred [41] [42] [43]. Owing to the steric hindrance and electrostatic repulsion between the two pairs of carboxylate groups, we believed that the coordination between COO^- and zinc ions possibly occurred through one oxygen of two pyromellitic acid molecules. The final product is a miscellaneous matter with multifunctional purpose.

3.2. Differential Scanning Calorimetry

Figure 3 displays the calorimetric curves of pyromellitic acid and TiP/EA modified with that acid, ZnAc and AgNO_3 . Pyromellitic acid showed crystallization (T_c) and melting (T_m) temperatures at 229 and 280 °C, respectively. T_m at 276 °C was reported at National Library of Medicine [44]. The sample TiP/EA/AP presented crystallization and melting peaks at 256 and 267 °C, respectively. The increase of T_c and the lowering of T_m were understood as the action of heterogeneous nucleation of the phosphate and the crystal formation with lesser thickness, respectively. Nonthermal event was noticed for the TiP/EA/AP/Zn and TiP/EA/AP/Zn/Ag samples. The absence of crystallization and melting peaks of pyromellitic acid in the samples modified with zinc and silver salts endorsed the deduction on the formation of zinc and silver carboxylate salts.

3.3. Wide Angle X-Ray Diffraction

Figure 4 shows diffraction patterns of the samples. WAXD of ZnAc presented a high intense diffraction angle at 12.8° and some others with lesser relevance [45] AgNO_3 registered low intensity diffraction angle at 21.9° and high intensity one in the vicinity of 36° [46] [47]. Pyromellitic acid revealed a series of diffraction angles which intensity followed this order: 11.75° and 25.95° > 16.0°, 24.9° and 31.95° > 29.1°. TiP indicated diffraction angles at 12.0° (hkl), like geminate at 21.25° - 22.35°, 26.0° and 35.65°. TiP/EA exhibited diffraction angles at 6.4°, 23.7°, 25.1° and 27.1°. Intercalation of zirconium and titanium phosphates is largely experienced [20] [48] [49] [50]. TiP/EA/AP presented intense diffraction angles at 5.5°, 22.05°, 23.05° and 27.0°. After intercalation with ZnAc, TiP/EA/AP/Zn

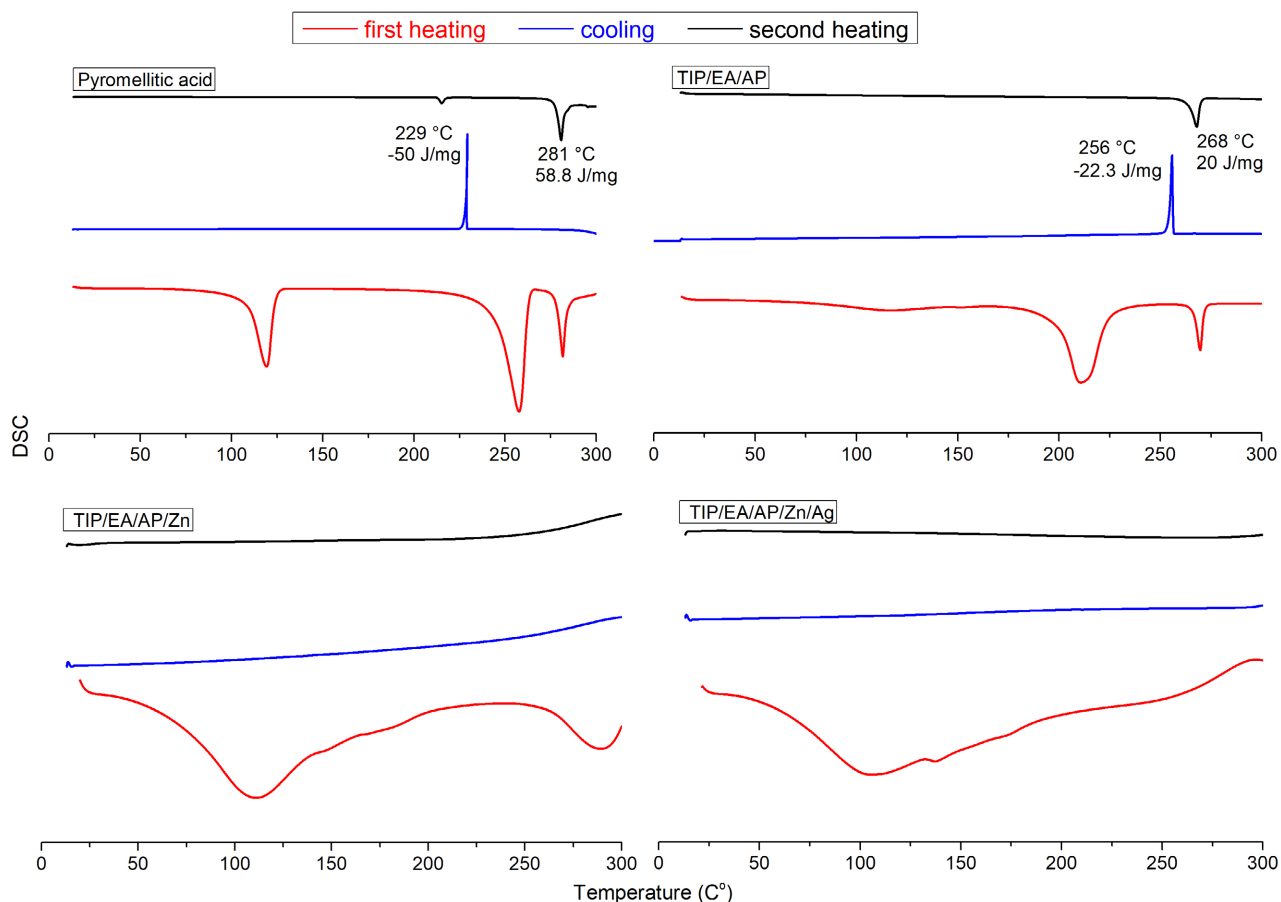


Figure 3. Calorimetric curves of pyromellitic acid and TiP/EA modified with pyromellitic acid, ZnAc and AgNO₃.

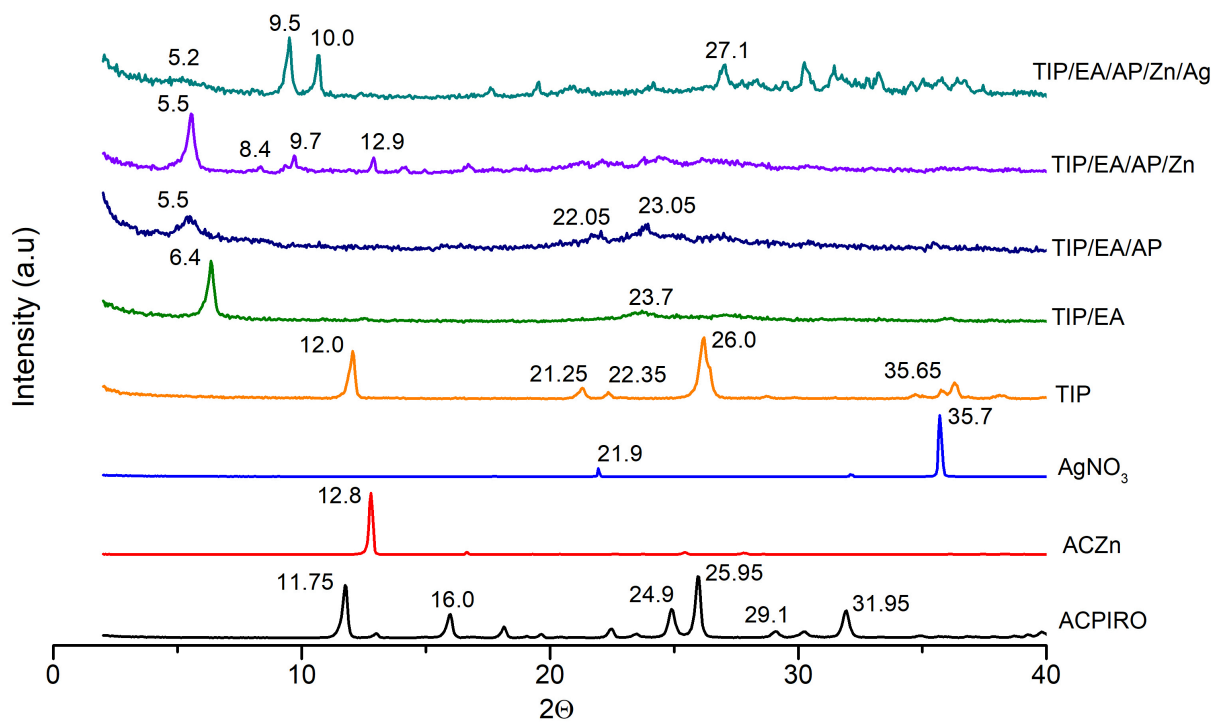


Figure 4. Diffraction patterns of pyromellitic acid, zinc acetate, AgNO₃, TIP, TIP/EA, TIP/EA/AP, TIP/EA/AP/Zn, TIP/EA/AP/Zn/Ag.

revealed diffraction angles at 5.5°, 8.4°, 9.7°, 12.9°, 22.1°, 24.4°, 26.2°. Lastly, TiP/EA/AP/Zn/Ag exhibited diffraction angles with high intensity at 5.2°, 9.5°, 10.0° and 27.0° and some others at 17.9°, 15.9°, 24.2°, 27.1°, 30.2°, 31.4°, 33.2°, 35.8°. Modification on the TiP arrangement was seen for each intercalation step. The addition of ethylamine provoked the disappearance of the TiP *hkl* crystalline plane and the other high angles practically vanished. A new diffraction angle at 6.4° emerged. These findings indicated that original TiP crystalline arrangement was perturbed forming an intercalated structure. After the incorporation of pyromellitic acid, there was the dislocation of the diffraction angle from 6.5° to 5.5°. The most diffraction angles of pyromellitic acid lost intensity. As seen in the DSC analysis, pyromellitic acid lowered its melting temperature. This brought about the decrease of crystal thickness bringing consequence in the intensity of the crystalline planes. The sample intercalated with ZnAc (TiP/EA/AP/Zn) showed a series of diffraction angles. The diffraction angle at 5.5° remained but new ones at 8.4° and 9.7° and 12.9° were observed. The addition of AgNO₃ induced great changes. The diffraction angle at 5.5° was partially displaced to 5.2°. The previous ones registered at 8.4° and 9.7° were shifted to 9.5° and 10.7°, respectively. That one at 12.9° disappeared but new diffraction angles from 15° emerged. Summarizing, to each step of intercalation there was changes in the TiP crystalline arrangement. The effect of ethylamine was emphatic. It entered inside TiP galleries forming an intercalating structure. We believed that the entrance of pyromellitic acid into the TiP/EA galleries induced the shift of the diffraction angle at 6.5° to low value meaning an increase of the lamellar spacing. The lesser intensity of pyromellitic acid diffraction peak could be associated to its difficulty to crystallize inside the TiP galleries. Partial intercalation was evidenced by addition of zinc salt. The new diffraction angles detected at 8.4° and 9.7° possibly appeared owing to the entrance of zinc salt and the ejection of some free pyromellitic acid. This could mean a reduction of its lamellar spacing. The diffraction angle at 12.9° was associated to the free molecules of ZnAc. We also speculated that a series of diffraction angles in the range of 14° - 25° could be related to formation of coordinate structures of pyromellitic acid and Zn ions. Strong diffraction peaks at 15.4°, 18.98° and 21.88° were reported by Yang *et al.* in their work on complexation of zinc ions and pyromellitic acid [35]. Also, they mentioned diffraction peaks at 11.26°, 19.62° and 22.55° related to the ZnAc. In the range of 5°-15°, the addition of AgNO₃ shifted the diffraction peaks to low and high values. In both cases, we believed that the accessibility of silver salt to the phosphate galleries was attained. Opposite effects were achieved meaning increase and decrease of lamellar spacing, respectively. Disappearance of the main crystalline plane of zinc salt (12.9°) suggested that some events could be happened such as the total or partial rejection of free ZnAc and/or the ions exchange with silver salt. The lowering in the intensity of the main diffraction angle of silver salt around 36° could be associated to silver coordination with free molecules of pyromellitic acid forming carboxylate salt or even its ion exchange with zinc acetate. The results endorsed the findings in FT-IR and DSC evaluations and

that a complex multifunctional miscellaneous matter was attained.

3.4. Field Emission Scanning Electron Microscope/Energy-Dispersive X-Ray Spectroscopy

Figure 5 displays the SEM images. ZnAc, AgNO₃ and pyromellitic acid showed agglomerated, fragmented, and shapeless structures. TiP micrograph revealed block of lamellae with hexagonal shape and heterogeneity of length and thickness.

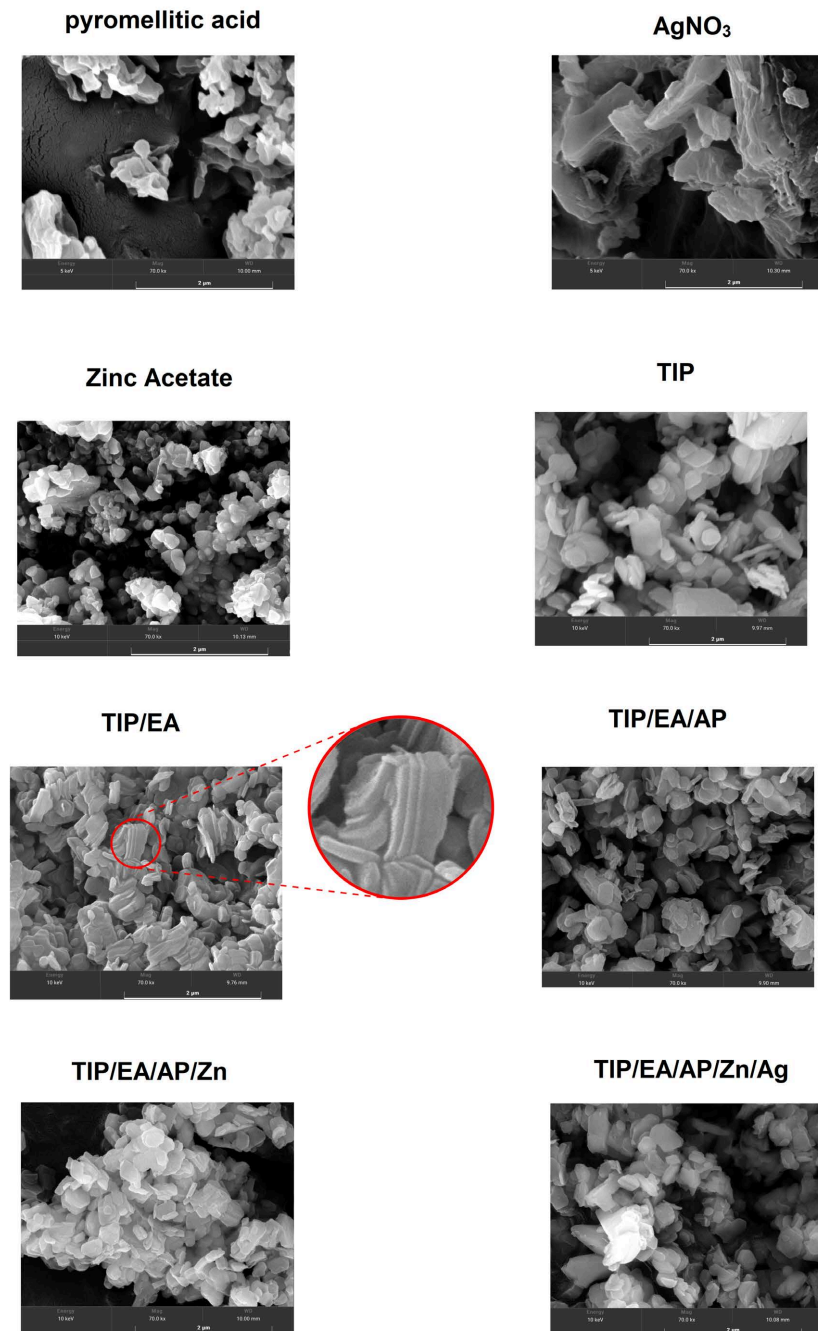


Figure 5. SEM images of pyromellitic acid, AgNO₃, ZnAc, TiP, TiP/EA TiP/EA/AP TiP/EA/AP/Zn and TiP/EA/AP/Zn/Ag.

Similarity was found for TiP/EA micrograph. Some of them showed the presence of intercalator among phosphate lamellae (highlighted image) provoking alteration of the spacing among phosphate lamellae. Tendency to delamination is clearly seen. TiP/EA/AP image induced to infer that the entrance of pyromellitic acid arouse higher level of delamination. For the TiP/EA/AP/Zn micrograph, the presence of ZnAc seems to have brought the agglomeration of the previous structures forming a kind of cluster. Possibly, these structures were built owing to the interaction of the outside P-O-H groups of phosphate and carbonyl group of zinc acetate. With the addition of AgNO₃, new fragmentation occurred but sharply the cluster deagglomeration was observed. It could mean that the interaction between P-O-H and carbonyl was disrupted possibly due to ion exchange between the zinc and silver salts. The results of the EDX analysis of the materials are shown in **Figure 6**. The TiP showed the energy peaks of Ti (4.93 keV, 4.5 keV and three peaks in the region 0.4 - 0.63 keV), P (2.0 keV) and O (5.2 keV). The ratios were equal to 54.8 wt% (74.66 at%), 24.72 wt% (17.15 at%) and 20.46 wt% (9.19 at%) for oxygen, phosphorous and Titanium, respectively. This result is in agreement with the literature. [51]. The energy peaks for the TiP/EA sample were of Ti (4.93 keV, 4.5 keV and three peaks in the region 0.4-0.63 keV), P (2.0 keV), O (5.2 keV), C (2.7 keV) and N (3.9 KeV). The ratios for the TiP/EA sample were equal to 42.98 wt% (48.64 at%), 17.81 wt% (10.41 at%), 14.33 wt% (5.42 at%), 15.75 wt% (23.74 at%) and 9.13 wt% (11.8 at%) for oxygen, phosphorous, titanium, carbon, and nitrogen respectively. The presence of carbon and nitrogen confirms the intercalation of ethylamine which agrees with the previous WAXD analysis. TiP/EA/AP sample showed energy peaks of Ti (4.93 keV, 4.5 keV and three peaks in the region 0.4 - 0.63 keV), P (2.0 keV), O (5.3 keV), C (2.8 keV) and N (3.9 KeV). The sample TIP/EA/AP show ratios of to 43.6 wt% (41.4 at%), 8.86 wt% (4.34 at%), 4.19 wt% (1.33 at%), 32.72 wt% (41.39 at%) and 10.63 wt% (11.53 at%) for oxygen, phosphorous, titanium, carbon, and nitrogen respectively. The increase in carbon in the sample TIP/EA/AP is a confirmation of the successful intercalation. The energy peaks of TIP/EA/AP/Zn were Ti (4.93 keV, 4.5 keV and three peaks in the region 0.4 - 0.63 keV), P (2.0 keV), O (5.2 keV), C (2.7 keV), N (3.9 KeV), Zn (8.6 and 9.5 keV), Al (1.4 keV) and Si (1.7 keV). The sample TIP/EA/AP/Zn contains 34.93 wt% (38.3 at%) of oxygen, 8.8 wt% (4.98 at%) of phosphorous, 8.31 wt% (3.05 at%) of titanium, 28.85 wt% (42.14 at%) of carbon, 6.38 wt% (7.99 at%) of nitrogen, 12.39 wt% (3.32 at%) of zinc, 0.16 wt% (0.11 at%) of aluminum and 0.18 wt% (0.11 at%) of silicon. As expected, the presence of zinc is confirmed in the sample which agrees with the WAXD analysis. The Sample TIP/EA/AP/Zn/Ag showed energy peaks of Ti (4.93 keV, 4.5 keV and three peaks in the region 0.4-0.63 keV), P (2.0 keV), O (5.2 keV), C (2.7 keV), N (3.9 KeV), Zn (8.6 and 9.5 keV), and Ag (2.9 keV, 3.1 keV, 3.3 keV, 3.5 keV). The sample TIP/EA/AP/Zn/Ag contains 31.99 wt% (42.01 at%) of oxygen, 8.31 wt% (5.63 at%) of phosphorous, 7.65 wt% (3.36 at%) of titanium, 20.5 wt% (35.86 at%) of carbon, 4.42 wt% (6.63 at%) of nitrogen, 9.7 wt% (3.11 at%) of zinc, and 17.44 wt% (3.4 at%) of silver. The analysis confirms

presence of silver confirming the intercalation. **Figure 7** shows schematically the effect of each intercalation on TiP galleries. When ethylamine was added (**Figure 7(a)**), the TiP original arrangement was modified and $d_{spacing}$ was increased. After

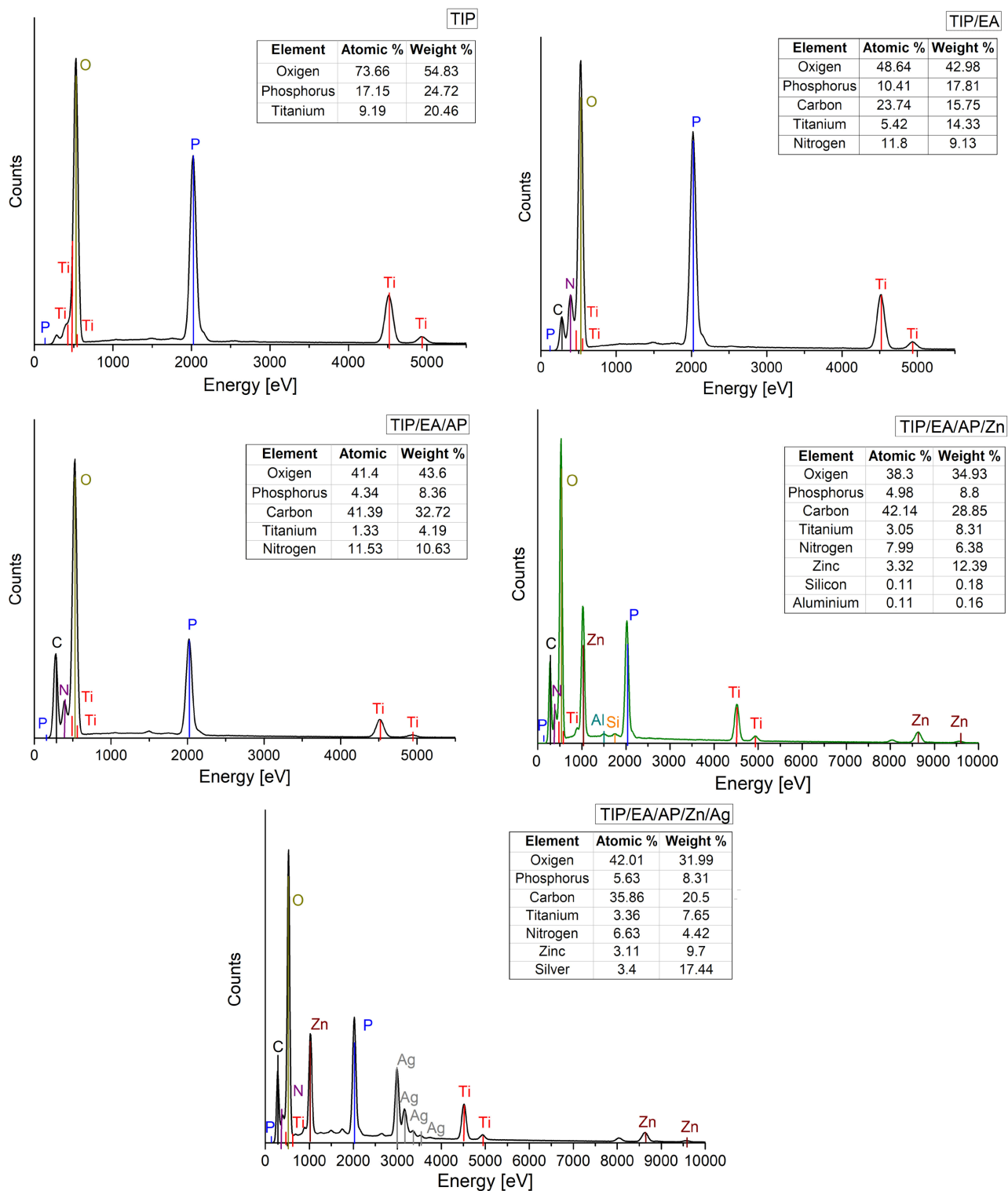


Figure 6. Energy dispersive X-ray spectrum of (a) TiP, (b) TiP/EA, (c) TiP/EA/AP (d) TiP/EA/AP/Zn and (e) TiP/EA/AP/Zn/Ag.

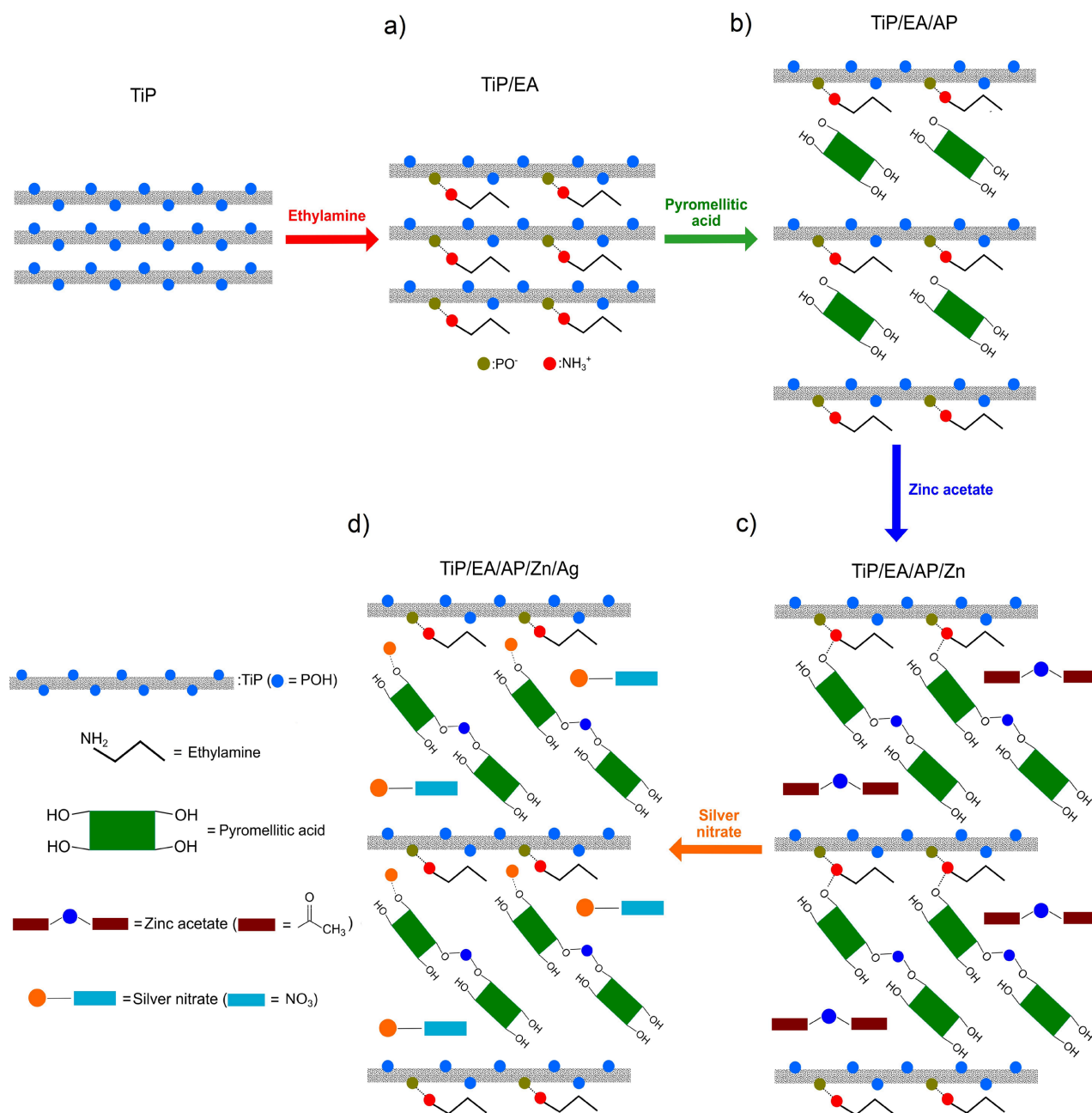


Figure 7. Schematic representation of each intercalation into TiP galleries.

addition of pyromellitic acid (Figure 7(b)), TiP/EA also showed the displacement of low diffraction angle to lower value resulting in higher d_{spacing} . The incorporation of ZnAc (Figure 7(c)) led mainly to the formation of zinc carboxylate, the interaction of free carboxyl groups with $\text{PO}^- \text{ } ^+\text{HN-CH}_2\text{CH}_3$ and the presence of free ZnAc. Finally, the addition of AgNO_3 (Figure 7(d)) induced the destruction of the interaction of free carboxyl groups with $\text{PO}^- \text{ } ^+\text{HN-CH}_2\text{CH}_3$, in some extent the displacement of low diffraction angle to lower value, the formation of zinc and silver carboxylates, the absence of ZnAc and the presence of free AgNO_3 .

3.5. Thermogravimetry

Figure 8 displays the TGA curves. In parenthesis is registered the loss mass in each degradation step. ZnAc presented two degradation steps. The first was assigned at 87°C (adsorbed water, 18%) and the second at 252°C (release of acetate moieties, 70%) similarly to found by Ghule and collaborators [52]. AgNO₃ exhibited two thermal degradation steps at 489°C and 530°C (38% and 2%). Jankovic *et al.* studied the non-isothermal decomposition of AgNO₃. They detected two thermal degradation steps at 468 and 508°C. The first was associated to the boiling following its decomposition. The second one was higher than its degradation finishing (around 500°C). The variation was related to the change in heat capacity [53]. Pyromellitic acid was degraded in two steps where the maximum occurred at 70°C (release of adsorbed water, 12%) and as geminated peaks at 258 and 269°C (acid degradation, 87%). Simultaneous thermoanalytical techniques ((TGA-DTG-DTA-ETA) were applied by Chiu to investigate thermal degradation of polyethylene oxide, pyromellitic acid, and polyacrylonitrile. Like found herein, it was reported that pyromellitic acid presented two decays of degradation (70°C-130°C and 180°C-260°C) [54]. TiP displays three steps of degradation. The first one ranged between 100°C - 150°C released of adsorbed water, 1%. The intermediary was between 150°C - 300°C (water in the crystalline lattice, 7%). The last one was around 400°C - 600°C (transformation of phosphate to pyrophosphate, 7%). TiP/EA exhibited five degradation decays. Below 100°C was released of residual solvent (9.7%). Between 100°C - 200°C represented the liberation of water adsorbed and linked to crystal lattice (4.6% and 2.1%). The last two (250°C - 400°C) were attributed to the release of amine free and linked (5.6% and 12.7%), respectively [20]. Four degradation steps were noticed for TiP/EA/AP. Below 100°C, it was detected the release of residual solvent (3.2%). In the range of 150°C - 280°C, maximum degradation peak was observed at 204°C (13%) and 235°C (15%). They were related to the structural degradation of aryl acid. The last degradation decay at 313°C (12%) was attributed to the release of amine linked as $\text{PO}^- \text{ }_3\text{HN-CH}_2\text{CH}_3$. Six degradation steps were seen for TiP/EA/AP/Zn. The first occurred at 43°C (6.9%) representing the release of residual solvent. A shoulder around 120°C (2.3%) was related to the adsorbed water. Sequentially, a new shoulder at the vicinity of 230°C (3.5%) was ascribed to the release of pyromellitic acid. The peak with maximum at 271°C (9.5%) denoted acetate moieties thermal degradation. Low intensity peak at 357°C (5.0%) described the thermal release of combined amine. We deduced that the middle intensity peak at 448°C (9.0%) represented the degradation of coordinate structures of pyromellitic acid and zinc ions. TiP/EA/AP/Zn/Ag revealed multiple degradation peaks. The initial peak at 45°C (7.6%) represented the release of residual solvent. In sequence, two shoulders appeared. Their assignments were around 230°C (2.3%) and 296°C (3.8%) describing degradation of free aryl acid and zinc acetate, respectively. The peak evidencing the release of the combined amine appeared at 334°C (7.5%). The last three peaks around 431°C, 530°C and

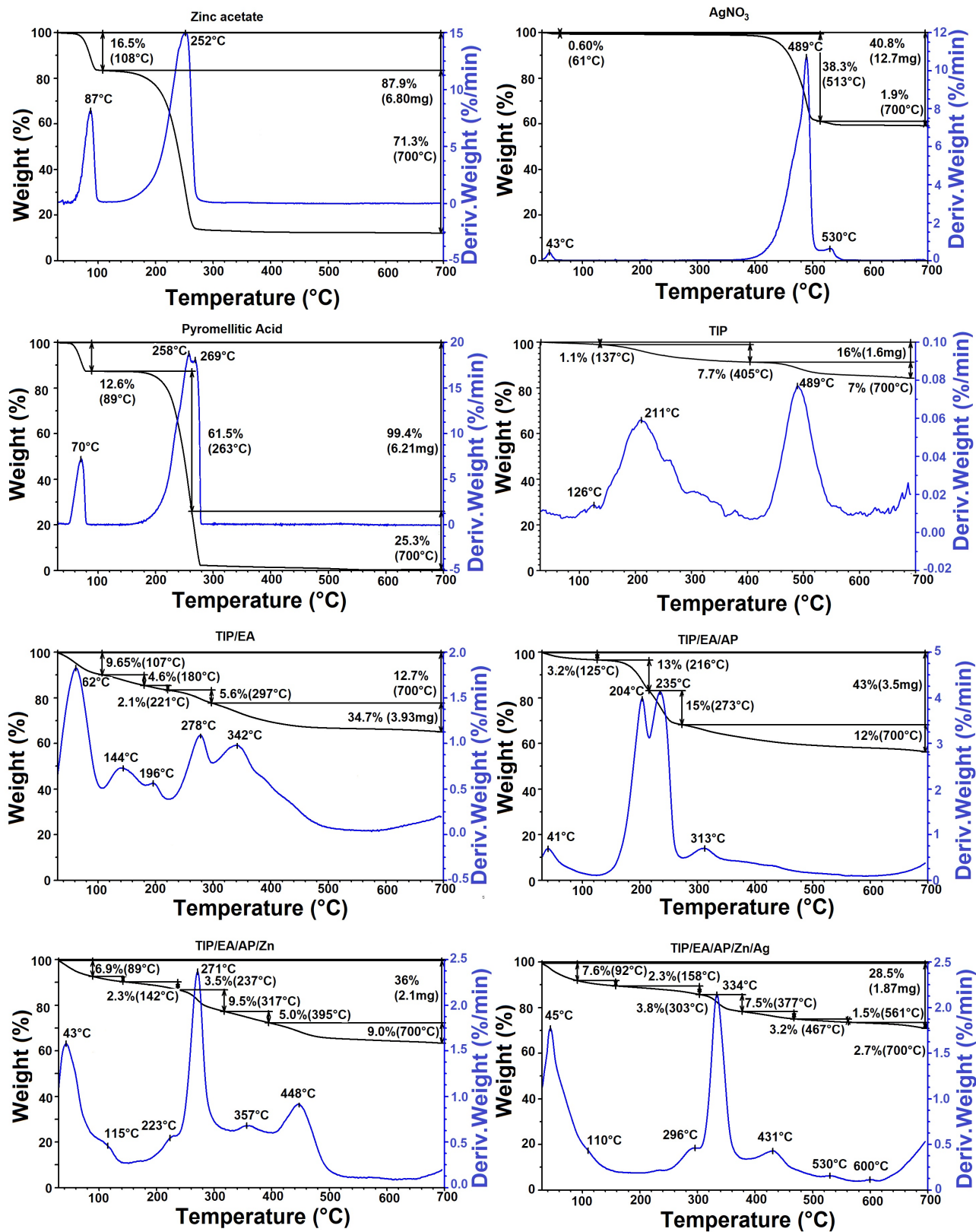


Figure 8. TGA and DTG curves of (a) zinc acetate (b) AgNO₃ (c) pyromellitic acid (d) TiP, (e) TiP/EA, (f) TiP/EA/AP (g) TiP/EA/AP/Zn and (h) TiP/EA/AP/Zn/Ag.

600 °C (3.2%, 1.5% and 2.7%) depicted the degradation of coordinate structures among pyromellitic acid, zinc, and silver ions. The results revealed herein corroborated those found in FTIR, WAXD, DSC, SEM. A complex multifunctional and miscellaneous matter was raised.

4. Conclusion

By using the lamellar structural arrangement of titanium phosphate, we intended to build a novel filler based on the properties of the zinc and silver matters. Consecutive intercalations were experienced. In each step changes in the TiP structural setting were noticed. Shifting and arising of infrared bands denoted changes in each step. For any kind of intercalator matter, TiP hexagonal array stacks were altered. When added, ZnAc and AgNO₃ revealed ability to build agglomerated and deagglomerated arrangements, respectively. Also, they reacted with free pyromellitic acid forming carboxylate salts increasing the phosphate thermal stability. The findings induced to deduce that the final miscellaneous and multifunctional matter presents great potential for application in polymeric nanocomposites.

Acknowledgements

Thanks to the Conselho Nacional de Desenvolvimento Científico e Tecnológico (CNPq) and Coordenação de Aperfeiçoamento de Pessoal de Nível Superior (CAPES) Finance Code 1 and Universidade Federal do Rio de Janeiro to support this research.

Conflicts of Interest

The authors declare no conflicts of interest regarding the publication of this paper.

References

- [1] Shankar, S., Wang, L.-F. and Rhim, J.-W. (2018) Incorporation of Zinc Oxide Nanoparticles Improved the Mechanical, Water Vapor Barrier, UV-Light Barrier, and Antibacterial Properties of PLA-Based Nanocomposite Films. *Materials Science and Engineering: C*, **93**, 289-298. <https://doi.org/10.1016/j.msec.2018.08.002>
- [2] Tabaii, M.J. and Emtiazi, G. (2018) Transparent Nontoxic Antibacterial wound Dressing Based on Silver Nano Particle/Bacterial Cellulose Nano Composite Synthesized in the Presence of Tripolyphosphate. *Journal of Drug Delivery Science and Technology*, **44**, 244-253. <https://doi.org/10.1016/j.jddst.2017.12.019>
- [3] Tamayo, L., Palza, H., Bejarano, J. and Zapata, P.A. (2019) Polymer Composites with Metal Nanoparticles: Synthesis, Properties, and Applications. In: Pielichowski, K. and Majka, T.M., Eds., *Polymer Composites with Functionalized Nanoparticles*, Elsevier, Amsterdam, 249-286. <https://doi.org/10.1016/B978-0-12-814064-2.00008-1>
- [4] Chu, Z., Zhao, T., Li, L., Fan, J. and Qin, Y. (2017) Characterization of Antimicrobial Poly (lactic acid)/Nano-Composite Films with Silver and Zinc Oxide Nanoparticles. *Materials*, **10**, Article 659. <https://doi.org/10.3390/ma10060659>
- [5] Al-Arfaj, A.A. and Soheir, N.A.E. (2021) Synthesis and Characterization of Zinc

- Oxide and Zinc Oxide Doped with Chlorine Nanoparticles as Novel α -Amylase Inhibitors. *Food and Nutrition Sciences*, **12**, 308-318. <https://doi.org/10.4236/fns.2021.123024>
- [6] Li, X., Natsuki, J. and Natsuki, T. (2021) Eco-Friendly Synthesis of Symmetrical Pyramid Structured Zinc Oxide Nanoparticles and High Temperature Stable UV-Shielding Properties of Zinc Oxide/Polyurethane Composite Membranes. *Physica E: Low-Dimensional Systems and Nanostructures*, **130**, Article ID: 114677. <https://doi.org/10.1016/j.physe.2021.114677>
- [7] Sheikh, M., Asghari, M. and Afsari, M. (2018) Effect of Tiny Amount of Zinc Oxide on Morphological and Thermal Properties of Nanocomposite PEBA Thin Films. *Alexandria Engineering Journal*, **57**, 3661-3669. <https://doi.org/10.1016/j.aej.2018.01.016>
- [8] Fiedot-Toboła, M., Ciesielska, M., Maliszewska, I.O., *et al.* (2018) Deposition of Zinc Oxide on Different Polymer Textiles and their Antibacterial Properties. *Materials*, **11**, Article 707. <https://doi.org/10.3390/ma11050707>
- [9] Zhou, B., Xu, B., Z., *et al.* (2018) Synthesis of Photoluminescent Zinc Acetate-Polyethylene Composite Coatings by Pulse Laser-Assisted Electron Beam Dispersion. *Journal of Materials Science*, **53**, 12214-12230. <https://doi.org/10.1007/s10853-018-2480-4>
- [10] Sionkowska, A., Walczak, M. and Michalska-Sionkowska, M. (2020) Preparation and Characterization of Collagen/Chitosan Composites with Silver Nanoparticles. *Polymer Composites*, **41**, 951-957. <https://doi.org/10.1002/pc.25426>
- [11] Rajabi, A., Ghazali, M.J., Mahmoudi, E., *et al.* (2019) Synthesis, Characterization, and Antibacterial Activity of Ag₂O-Loaded Polyethylene Terephthalate Fabric via Ultrasonic Method. *Nanomaterials*, **9**, Article 450. <https://doi.org/10.3390/nano9030450>
- [12] Tan, S.-J., Yue, J., Tian, Y.-F., Ma, Q., Wan, J., Xiao, Y., Zhang, J., Yin, Y.-X., Wen, R. and Xin, S. (2021) *In-Situ* Encapsulating Flame-Retardant Phosphate into Robust Polymer Matrix for Safe and Stable Quasi-Solid-State Lithium Metal Batteries, Energy Storage. *Materials*, **39**, 186-193. <https://doi.org/10.1016/j.ensm.2021.04.020>
- [13] Huang, H., Li, M., Tian, Y., Xie, Y., Sheng, X., Jiang, X. and Zhang, X. (2020) Exfoliation and Functionalization of α -Zirconium Phosphate in One Pot for Waterborne Epoxy Coatings with Enhanced Anticorrosion Performance. *Progress in Organic Coatings*, **138**, Article ID: 105390. <https://doi.org/10.1016/j.porgcoat.2019.105390>
- [14] Salama, A. (2019) Cellulose/Calcium Phosphate Hybrids: New Materials for Biomedical and Environmental Applications. *International Journal of Biological Macromolecules*, **127**, 606-617. <https://doi.org/10.1016/j.ijbiomac.2019.01.130>
- [15] Wang, C., Cheng, Q. and Wang, Y. (2018) Anion-Controlled Cation-Exchange Process: Intercalating α -Titanium Phosphate through Direct Ion Exchange with Alkylammonium Salts. *Inorganic Chemistry*, **57**, 3753-3760. <https://doi.org/10.1021/acs.inorgchem.7b03030>
- [16] Kraus, K.A. and Phillips, H.O. (1956) Adsorption on Inorganic Materials. I. Cation Exchange Properties of Zirconium Phosphate. *Journal of the American Chemical Society*, **78**, 694. <https://doi.org/10.1021/ja01584a053>
- [17] Alberti, G., Cardini-Galli, P., Costantino, U. and Torracca, E. (1967) Crystalline Insoluble salts of Polybasic Metals-I Ion-Exchange Properties of Crystalline Titanium Phosphate. *Journal of Inorganic and Nuclear Chemistry*, **29**, 571-578. [https://doi.org/10.1016/0022-1902\(67\)80063-0](https://doi.org/10.1016/0022-1902(67)80063-0)
- [18] Espina, A., García, J.R., Guil, J.M., Jaimez, E., Parra, J.B. and Rodríguez, J. (1998)

- Calorimetric Study of Amine Adsorption on α - and γ -Titanium Phosphate. *The Journal of Physical Chemistry B*, **102**, 1713-1716. <https://doi.org/10.1021/jp972410o>
- [19] Nunes, L.M. and Airoidi, C. (2000) The Intercalation of Some Heterocyclic Amines Into α -Titanium Hydrogenphosphate—Structural and Calorimetric Data. *Journal of Solid State Chemistry*, **154**, 557-563. <https://doi.org/10.1006/jssc.2000.8879>
- [20] Albitres, G.A., Cestari, S.P., Freitas, D.F., Rodrigues, D.C., Mendes, L.C. and Neumann, R. (2020) Intercalation of α -Titanium Phosphate with Long-Chain Amine Aided by Short-Chain Amine. *Applied Nanoscience*, **10**, 907-916. <https://doi.org/10.1007/s13204-019-01176-1>
- [21] García-Glez, J., Trobajo, C., Khainakov, S.A. and Amghouz, Z. (2017) α -Titanium Phosphate Intercalated with Propylamine: An Alternative Pathway for Efficient Europium(III) Uptake into Layered Tetravalent Metal Phosphates. *Arabian Journal of Chemistry*, **10**, 885-894. <https://doi.org/10.1016/j.arabjc.2016.07.013>
- [22] García, I., Trobajo, C., Amghouz, Z. and Adawy, A. (2021) Nanolayered Metal Phosphates as Biocompatible Reservoirs for Antimicrobial Silver Nanoparticles. *Materials*, **14**, Article 1481. <https://doi.org/10.3390/ma14061481>
- [23] Ren, M., Bao, J., Wang, P., Wang, C. and Ao, Y. (2018) Titanium Phosphate Nanoplates Modified with AgBr@Ag Nanoparticles: A Novel Heterostructured Photocatalyst with Significantly Enhanced Visible Light Responsive Activity. *Frontiers in Chemistry*, **6**, Article 489. <https://doi.org/10.3389/fchem.2018.00489>
- [24] Clearfield, A., Blessing, R.H. and Stynes, J.A. (1968) New Crystalline Phases of Zirconium Phosphate Possessing Ion-Exchange Properties. *Journal of Inorganic and Nuclear Chemistry*, **30**, 2249-2258. [https://doi.org/10.1016/0022-1902\(68\)80224-6](https://doi.org/10.1016/0022-1902(68)80224-6)
- [25] Tegehall, P.-E. (1986) Synthesis of Crystalline Titanium(IV) Phosphates by Direct Precipitation from Ti(III) Solutions and Ion Exchange Properties of Some of the Prepared Phases. *Acta Chemica Scandinavica*, **40**, 507-514. <https://doi.org/10.3891/acta.chem.scand.40a-0507>
- [26] ASTM (2015) D3418-03 Standard Test Method for Transition Temperatures and Enthalpies of Fusion and Crystallization of Polymers by Differential Scanning Calorimetry. ASTM International, West Conshohocken, PA.
- [27] Pouchert, C.J. (1985) The Aldrich Library of FT-IR Spectra. Vol. 2, Aldrich Chemical Company, Milwaukee, 1275.
- [28] Augustine, R., Kalarikkal, N. and Thomas, S. (2014) A Facile and Rapid Method for the Black Pepper Leaf Mediated Green Synthesis of Silver Nanoparticles and the Antimicrobial Study. *Applied Nanoscience*, **4**, 809-818. <https://doi.org/10.1007/s13204-013-0260-7>
- [29] Pretsch, E., Bühlmann, P., Affolter, C., and Affolter, C. (2000) Structure Determination of Organic Compounds. Springer, Berlin. <https://doi.org/10.1007/978-3-662-04201-4>
- [30] Silverstein, R.M., Webster, F.X. and Kiemle, D.J. (2005) Spectrometric Identification of Organic Compounds. John Wiley & Sons, Hoboken.
- [31] Mishra, M. (2016) Fourier Transform Infrared Spectrophotometry Studies of Chromium Trioxide-Phthalic Acid Complexes. *Chemical Science Transactions*, **5**, 770-774. <https://doi.org/10.7598/cst2016.1260>
- [32] <https://pubchem.ncbi.nlm.nih.gov/compound/Pyromellitic-acid>
- [33] Bao, C.L., Song, L., Guo, Y. and Hu, Y. (2011) Preparation and Characterization of Flame-Retardant Polypropylene/ α -Titanium Phosphate (Nano)Composites. *Polymers for Advanced Technologies*, **22**, 1156-1165.

- <https://doi.org/10.1002/pat.1976>
- [34] Peng, W.J., Wang, X.G., Wang, M.M., Wang, Y.J. and Cheng, Q.Y. (2020) Embedding Alkyldiamine into Layered α -Titanium Phosphate via Direc-Ion Exchange and its Application in Eu^{III} Removal from Water. *Zeitschrift für anorganische und allgemeine Chemie*, **646**, 399-406. <https://doi.org/10.1002/zaac.201900349>
- [35] Yang, R.-G., Wang, M.-L., Liu, T. and Zhong, G.-Q. (2018) Room Temperature Solid state Synthesis, Characterization, and Application of a Zinc Complex with Pyromellitic Acid. *Crystals*, **8**, Article 56. <https://doi.org/10.3390/cryst8020056>
- [36] Qin, W., Xin, Z., Pan, C., Sun, S., Jiang, X. and Zhao, S. (2019) *In Situ* Formation of Zinc Phthalate as a Highly Dispersed β -Nucleating Agent for Mechanically Strengthened Isotactic Polypropylene. *Chemical Engineering Journal*, **358**, 1243-1252. <https://doi.org/10.1016/j.cej.2018.10.108>
- [37] Loring, J.S., Karlsson, M., Fawcett, W.R. and Casey, W.H. (2001) Infrared Spectra of Phthalic Acid, the Hydrogen Phthalate Ion, and the Phthalate Ion in Aqueous Solution. *Spectrochimica Acta Part A: Molecular and Biomolecular Spectroscopy*, **57**, 1635-1642. [https://doi.org/10.1016/S1386-1425\(01\)00391-2](https://doi.org/10.1016/S1386-1425(01)00391-2)
- [38] Suh, J.S. and Kim, J. (1998) Three Distinct Geometries of Surface-Adsorbed Carboxylate Groups. *Journal of Raman spectroscopy*, **29**, 143-148.
- [39] Joo, S.W., Han, S.W., Han, H.S. and Kim, K. (2000) Adsorption and Stability of Phthalic acid on a Colloidal Silver Surface: Surface-Enhanced Raman Scattering Study. *Journal of Raman Spectroscopy*, **31**, 145-150.
- [40] Smith, B.C. (2020) Organic Nitrogen Compounds VIII: Imides. *Journal of Spectroscopy*, **35**, 26-30.
- [41] Khadiran, N.F., Hussein, M.Z., Ahmad, R., *et al.* (2021) Preparation and Properties of Zinc Layered Hydroxide with Nitrate and Phosphate as the Counter Anion, A Novel Control Release Fertilizer Formulation. *Journal of Porous Materials*, **28**, 1797-1811. <https://doi.org/10.1007/s10934-021-01122-z>
- [42] http://www.hanhonggroup.com/ir/ir_en/RE01010195.html
- [43] http://www.hanhonggroup.com/ir/ir_en/RA10590005.html
- [44] <https://pubchem.ncbi.nlm.nih.gov/compound/Pyromellitic-acid>
- [45] Aarii, T. and Kishi, A. (2003) The Effect of Humidity on Thermal Process of Zinc Acetate. *Thermochimica Acta*, **400**, 175-185. [https://doi.org/10.1016/S0040-6031\(02\)00487-2](https://doi.org/10.1016/S0040-6031(02)00487-2)
- [46] Hou, Y., Pan, Y., Dong, C. and Nie, B. (2020) Direct Transformation of AgNO_3 Complex Encapsulated Fullerene (C_{60}) Microcrystal on Solid Silver Nitrate Crystal without Organic Ligands. *Applied Organometallic Chemistry*, **34**, e5978. <https://doi.org/10.1002/aoc.5978>
- [47] Aziz, S.B., Abdulwahid, R.T., Rasheed, M.A., Abdullah, O.G. and Ahmed, H.M. (2017) Polymer Blending as a Novel Approach for Tuning the SPR Peaks of Silver Nanoparticles. *Polymers*, **9**, Article 486. <https://doi.org/10.3390/polym9100486>
- [48] Ramos-Garcés, M.V., González-Villegas, J., López-Cubero, A. and Colón, J.L. (2021) New Applications of Zirconium Phosphate Nanomaterials. *Accounts of Materials Research*, **2**, 793-803. <https://doi.org/10.1021/accountsmr.1c00102>.
- [49] Zhang, J., Feng, L., Jian, Y., Luo, G., Wang, M., Hu, B., Liu, T., Li, J., Yuan, Y. and Wang, N. (2022) *cof* Uranium Contamination in Radioactive Effluent. *Chemical Engineering Journal*, **429**, Article ID: 132265. <https://doi.org/10.1016/j.cej.2021.132265>
- [50] Mariano, D.D.M., Freitas, D.D.F.D.S. and Mendes, L.C. (2021) Nano Lamellar Zir-

conium Phosphate and Screw Speed Changing Properties of Melt Extrusion Polypropylene Nanocomposites. *Journal of Composite Materials*, **55**, 2443-2458. <https://doi.org/10.1177/0021998320988758>

- [51] Liu, Z., Feng, Y. and Li, H. (2021) Application of Titanium Phosphate Prepared from Acidic Titanium Dioxide Wastewater to Remove Cerium(III) in Aqueous Solution. *Colloids and Surfaces A: Physicochemical and Engineering Aspects*, **630**, Article ID: 127613. <https://doi.org/10.1016/j.colsurfa.2021.127613>
- [52] Ghule, A.V., Lo, B., Tzing, S.H., Ghule, K., Chang, H. and Ling, Y.C. (2003) Simultaneous Thermogravimetric Analysis and *in Situ* Thermo-Raman Spectroscopic Investigation of Thermal Decomposition of Zinc Acetate Dihydrate Forming Zinc oxide Nanoparticles. *Chemical Physics Letters*, **381**, 262-270. <https://doi.org/10.1016/j.cplett.2003.09.125>
- [53] Janković, B., Stopić, S., Bogović, J. and Friedrich, B. (2014) Kinetic and Thermodynamic Investigations of Non-Isothermal Decomposition Process of a Commercial Silver Nitrate in an Argon Atmosphere Used as the Precursors for Ultrasonic Spray Pyrolysis (USP): The Mechanistic Approach. *Chemical Engineering and Processing: Process Intensification*, **82**, 71-87. <https://doi.org/10.1016/j.cep.2014.06.002>
- [54] Chiu, J. (1967) Technique for Simultaneous Thermogravimetric, Derivative thermogravimetric, Differential Thermal, and Electrothermal Analyses. *Analytical Chemistry*, **39**, 861-867. <https://doi.org/10.1021/ac60252a042>